CHAPTER 3

MATERIALS AND METHODOLOGIES

This chapter discusses the detail of the materials and software or simulation tools used in this work. The methods opted for evaluation and analyses of the results are also discussed. ***Section 3.1*** *of this chapter illustrates the step-by-step processes followed in this work. Various simulation tools and software used to carry out the modeling and analysis in this work are described.* ***Section 3.2*** *provides the details of the process work flow in the study of the soiling effect on PV performance and their correlation with the environmental parameters. In* ***section 3.3****, the instruments, their specifications and set-up while conducting the experiments are also mentioned. The flow of the overall work process of this research work is shown in a block diagram below (Figure 3.1).*

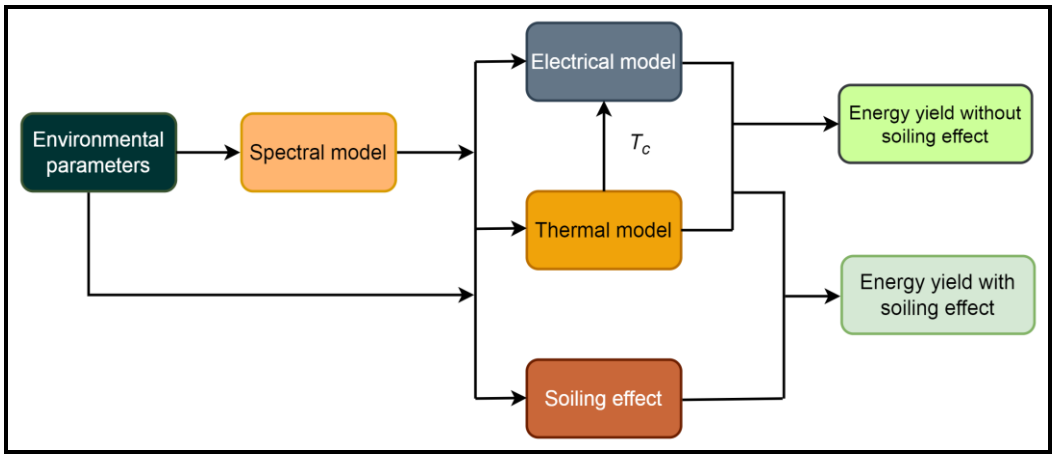

Figure 3.1 The overall flow of the work with three models, namely spectral, electrical, and thermal models along with the effect of soiling.

3.1 Spectral, electrical, and thermal modeling

The accurate performance of the PV module can be predicted with an integrated approach of solar irradiance, spectrum, thermal effect and electrical modeling. This section consists of three subsections, spectral modeling: the generation of the solar spectrum, electrical modeling: a model developed to analyze the electrical performance; and thermal modeling: a model developed to investigate the temperature

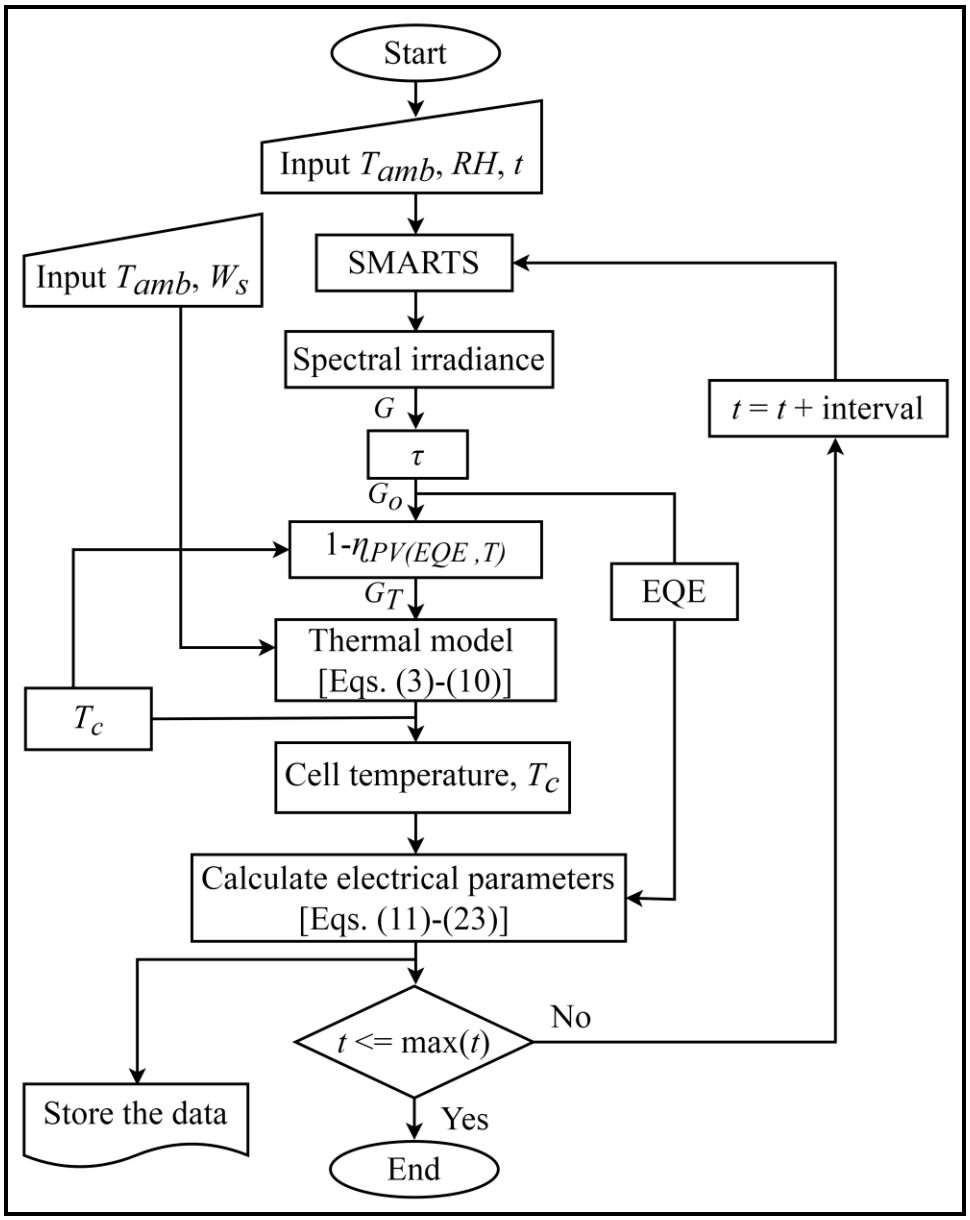

Figure 3.2 Flowchart of model development. Here T_{amb}: ambient temperature, *RH*: relative humidity, *t*: time, W_s: wind speed, τ: transmittance, *EQE*: external quantum efficiency, and T_c: cell temperature.

distribution. These three models are then integrated to determine the output of a PV module. A spectrum-based integrated thermal and electrical model to estimate the PV module output is developed for the evaluation of the performance of the PV module under transient conditions. The model considers the real-time variation of environmental parameter, solar spectrum, and cell temperature. Figure 3.2 illustrates the process flow of the model. As can be seen, the model consists of three parts, solar

spectrum generation, thermal modeling, and electrical modeling. The part of the solar spectrum absorbed by the solar cells generates electricity; however, because of the spectral response of the solar cells, which is a function of wavelength, not the entire absorbed solar spectrum gets converted to electricity. The portion of the solar spectrum which is not used in electricity generation contributes to heat generation [60]. Heating up of the PV module decreases its efficiency, attributed to the increase in the recombination rates of the internal carrier with an increase in the concentration of the minority carriers as the temperature rises [151]. Thus, it is important to evaluate the temperature distribution on the performance of the PV; therefore, thermal modeling has been considered. Moreover, in outdoor conditions, cell temperature, spectral irradiance, and environmental parameters are dynamic. These parameters are fed as an input for an instant of time *t* to the electrical model to obtain a more precise power output, and the individual models (spectral model, thermal model, and electrical model) are integrated using the COMSOL Multiphysics 5.4 Matlab Livelink module. Overall, the module uses simple mathematical equations to precisely estimate the seasonal, diurnal power output and energy yield of the PV modules.

3.1.1 Solar spectrum modeling

The solar spectrum is generated using the Simple Model of the Atmospheric Radiative Transfer of Sunshine version 2.9.5 (SMARTSv2.9.5) [94, 217]. SMARTSv2.9.5 is a tool that has been used successfully by many researchers to generate the solar spectrum using atmospheric parameters as input for a specific site [89, 218, 219]. It is an open-access tool provided by National Renewable Energy Laboratory (NREL), USA [220]. The snapshot of the tool with various input configurations is shown in Figure 3.3.

This tool generates the solar spectrum of a location based on the inputs latitude, altitude, height, and pressure of the site; various atmospheric parameters (either by selecting the defined reference atmosphere or non-reference atmosphere, which is user defined). Water vapor, ozone, gaseous absorption (concentration of pollutants), and carbon dioxide concentrations are also some of the input configurations. There are other configurations, such as extraterrestrial spectrum,

aerosol model, turbidity value, albedo, and spectral ranges, which can be set as per the requirement. Optionally, the

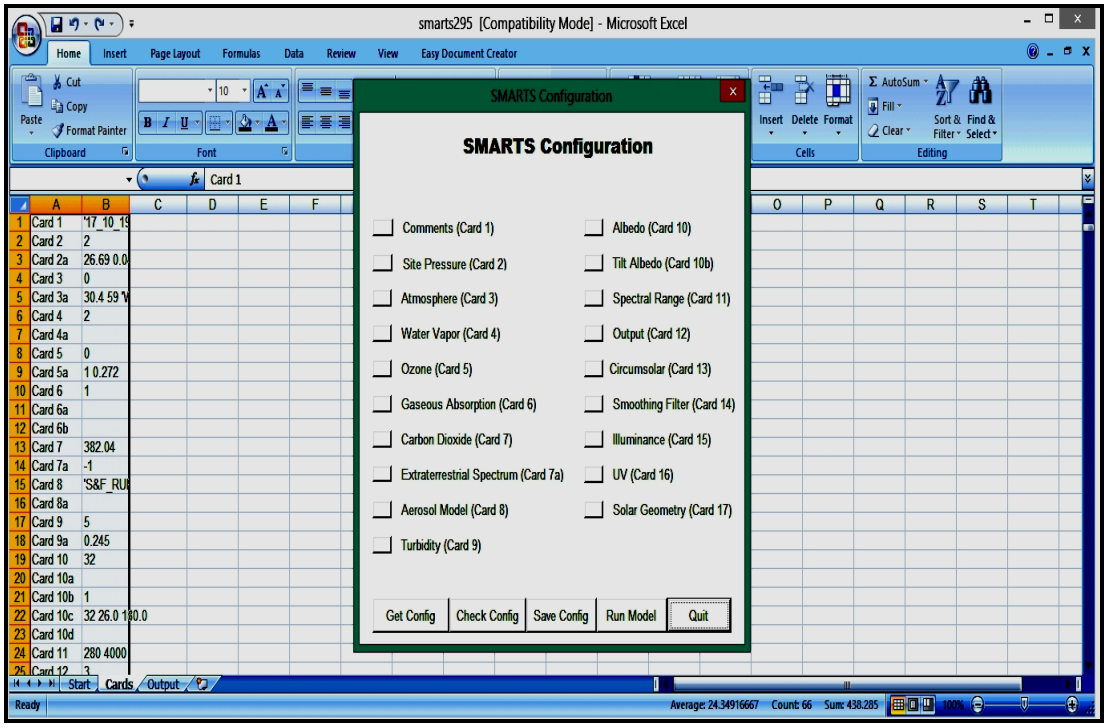

Figure 3.3 Snapshot of the SMARTSv2.9.5 with the input configurations to generate the solar spectral irradiance of a site.

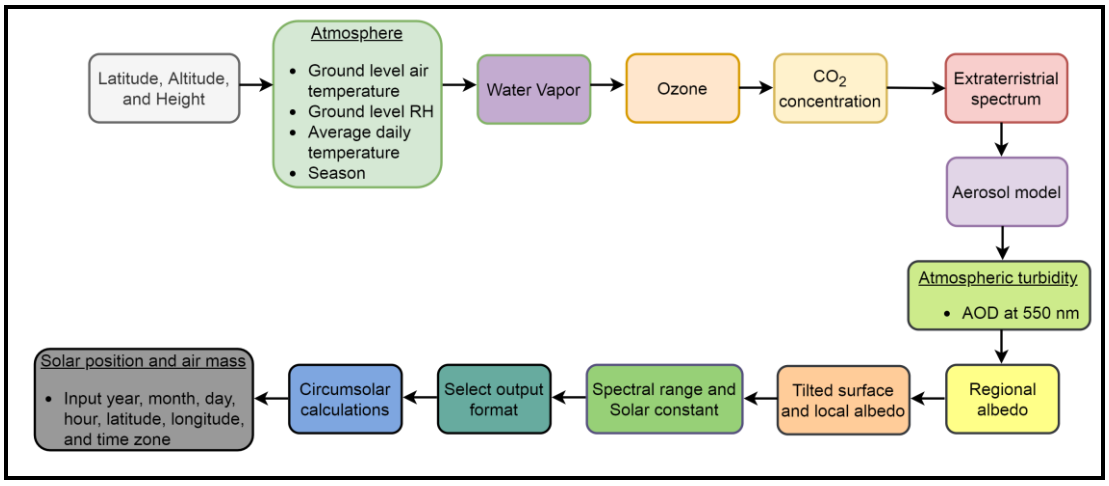

Figure 3.4 The step-by-step process in SMARTSv2.9.5.

geometry of the radiometer can also be fed to the input. The solar position and air mass value of the required site can be defined. The step-by-step input of the component is shown in Figure 3.4.

Here, the latitude, altitude, and height are defined as 26.69° North, 0.047 km at the ground, and 0.006 km above ground, respectively. The environmental parameters: relative humidity (*RH*), ambient temperature (T_{amb}), and daily temperature values are set to diurnal change. The ozone level, carbon dioxide concentration, and turbidity level at Aerosol Optical Depth (AOD) 550 nm used are average seasonal value accessed from NASA SSE [221] and is presented in Table 3.1. The model considers Shettle and Fenn's rural aerosol with regional albedo of light loam. A fixed tilt surface of 26° and 180° azimuth angle (south facing) is considered to represent the experimental setup. Under circumsolar calculations the radiometer geometry, the slope, aperture/opening and limit are set as 0, 2.5, and 0, respectively. The solar geometry configuration input of the year, month, day, hour, latitude, longitude, and time zone for the considered site.

Table 3.1 The seasonal value of the environmental parameters input to SMARTSv2.9.5 during various seasons.

Parameters	**Winter**	**Pre-monsoon**	**Monsoon**	**Post-monsoon**
Ozone level (atm-cm)	0.26	0.28	0.27	0.26
Carbon dioxide concentration (ppm)	382.76	382.79	382.04	382.43
Turbidity level at AOD 550 nm	0.27	0.69	0.25	0.25

The total spectral irradiance obtained from the spectral model strikes the surface of the front glass cover, and not all the solar spectrum gets transmitted; this is because of the partial reflection and absorption phenomena. When the modules are mounted at a fixed tilt, transmittance loss occurs (especially during the time of sunrise and sunset), which is attributed to the dependence of transmittance on the angle of incidence of the sun's ray. Therefore, the total absorbed solar spectrum (G_o) by the solar cells is calculated as follows:

$$G_o = G\,\tau \tag{3.1}$$

where G is the total incident solar spectrum (W/m^2) generated using SMARTS and τ is the transmittance of the front glass cover, equated as [222]:

$$\tau = \tau_{reflec}\ \tau_{absor} \tag{3.2}$$

where τ_{reflec} and τ_{absor} are transmittances due to the reflection of radiation and absorption of glazing. The transmittance due to reflection components can be obtained as follow:

$$\tau_{reflec} = \frac{1}{2}\left(\frac{1-\dfrac{\tan^2(\theta_2-\theta_1)}{\tan^2(\theta_2+\theta_1)}}{1+\dfrac{\tan^2(\theta_2-\theta_1)}{\tan^2(\theta_2+\theta_1)}} + \frac{1-\dfrac{\sin^2(\theta_2-\theta_1)}{\sin^2(\theta_2+\theta_1)}}{1+\dfrac{\sin^2(\theta_2-\theta_1)}{\sin^2(\theta_2+\theta_1)}} \right) \tag{3.3}$$

where θ_1 and θ_2 are the angles of incidence and refraction, respectively. At normal incidence, the angles θ_1 and θ_2 are equal to zero. Therefore, equation (3.3) for the normal incidence can be written as:

$$\tau_{reflec} = \left(\frac{n_1 - n_2}{n_1 + n_2} \right)^2 \tag{3.4}$$

These angles are related, according to Snell's law,

$$n_1 \sin\theta_1 = n_2 \sin\theta_2 \tag{3.5}$$

where n_1 and n_2 are the refractive indices of air and glass, respectively. Here the n_1 is considered to be 1, and n_2 is equal to 1.526. The angle of incidence θ_1 can be calculated using the equation given by [222]:

$$\theta_1 = \cos^{-1}\begin{pmatrix} \sin\delta\sin\phi\cos\beta - \sin\delta\cos\phi\sin\beta\cos\gamma + \cos\delta\cos\phi\cos\beta\cos\omega \\ + \cos\delta\sin\phi\sin\beta\cos\gamma\cos\omega + \cos\delta\sin\beta\sin\gamma\sin\omega \end{pmatrix} \tag{3.6}$$

where δ is the declination angle, ω is the hour angle, φ, β and γ are the latitude, slope, and surface azimuth angle, respectively.

$$\delta = 23.45^{\circ} \sin\left(284 + d\,\frac{360}{365} \right) \tag{3.7}$$

where d is the i^{th} day of the year.

The transmittance due to absorption components is expressed as:

$$\tau_{absor} = \exp\left(-\frac{KL_p}{\cos\theta_2}\right) \tag{3.8}$$

where K and L_p are the extinction coefficient and path length, respectively. K is considered to be 1 m^{-1}, and L is 0.32 cm.

The transmitted solar spectrum is received by the solar cells of the PV module; however, due to the spectral response (function of wavelength) of the solar cell, total transmitted spectral irradiance does not get used in electricity generation by the solar cells. The definitions of the spectral response (SR) and external quantum efficiency (EQE) and their correlation are provided in section 1.5 of chapter 1. *EQE* value as a function of wavelength for the two types of solar cells, monocrystalline (m-Si) and polycrystalline (p-Si), which is considered in this work, is shown in Figure 3.5.

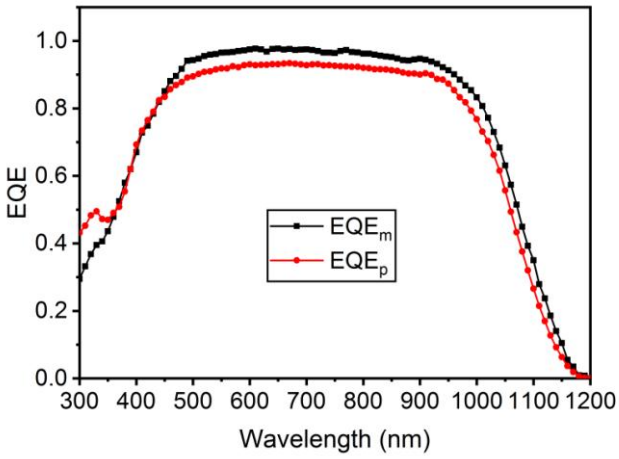

Figure 3.5 The external quantum efficiency (EQE) of the monocrystalline and polycrystalline silicon solar cells. Subscripts '*m*' and '*p*' denote the monocrystalline and polycrystalline, respectively [32].

The other part of the solar spectrum, which is received by the solar cells of the PV module, however, does not get used in electricity generation, leading to heat generation in the PV module attributed to the rise in temperature. Therefore, to estimate the temperature distribution due to diurnal spectral variation and

environmental parameters, the power to the thermal model is calculated using the equation:

$$P_o = G_T \, A \tag{3.9}$$

where G_T is the total irradiance (W/m^2) that contributes to heat generation in the PV module, A is the active area of the solar cells (m^2), and the total irradiance that contributes to heat generation, G_T is given by the equation [89]:

$$G_T = G_o\left(1 - \eta_{PV(EQE,\,T)}\right) \tag{3.10}$$

where $\eta_{PV(EQE,T)}$ is the efficiency of the PV module, depending on the EQE (function of wavelength λ) and cell temperature at an instant of time *t*, and is expressed as [57]:

$$\eta_{PV(EQE,T)} = \eta_{PV(EQE,T)t=0}[1 - K_v(T_c - T_r)] \tag{3.11}$$

where $\eta_{PV(EQE,\,T)t=0}$ is the efficiency at the initial conditions. K_v represents the temperature coefficient, T_c is the cell temperature (°C), and T_r is the reference temperature (°C).

3.1.2 Thermal modeling

The spectrum-based 3D thermal model has been developed in system HP Z238 Microtower Workstation Intel® Xenon ® CPU E3-1240 v6@ 3.70GHz, 32GB RAM, 64-bit operating system, x64-based processor using COMSOL Multiphysics version 5.4 with heat transfer module. The step-by-step process in COMSOL Multiphysics is shown in Figure 3.6.

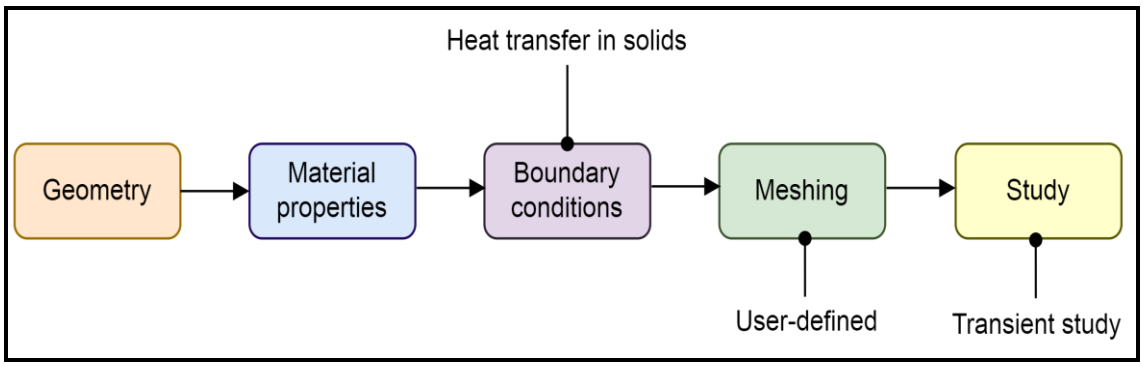

Figure 3.6 Steps followed in COMSOL Multiphysics.

Firstly, the geometry of the PV module consisting of different components in the sequence of top to bottom is as follows glass, ethylene-vinyl acetate (EVA) sheet, solar cells, EVA sheet, and backsheet (back surface) surrounded with aluminium metal frame has been designed (as shown in Figure 3.7) with the dimensions of each.

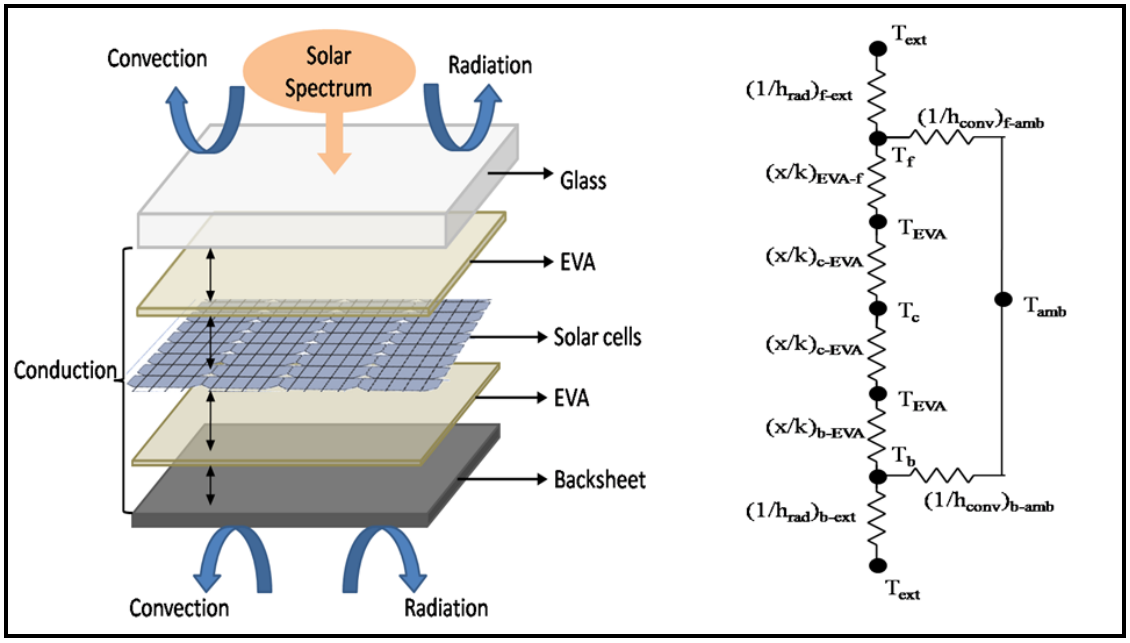

Figure 3.7 Different layers with various modes of heat transfer (left) and thermal network (right) of PV module. *x* is the thickness, *k* is the conduction heat transfer coefficient, and *h* represents the heat transfer coefficient. Subscripts *f*, *c*, *b*, *amb*, *conv*, *rad*, *ext*, and EVA denotes front, cell, back, ambient, convection, radiation, external, and ethylene-vinyl acetate, respectively.

component depicted in Table 3.2. The dimensions are predetermined to match those of the PV modules used for validations. The geometry of the modeled m-Si and p-Si PV modules are shown in the Figures 3.8(a) and (c), respectively. The photographs of the m-Si and p-Si PV modules that are used in experimental campaign and have same dimensions as modeled PV modules are shown in Figures 3.8(b) and (d), respectively. Since the contacts, fingers, and busbars have minimal impact on the thermal aspect of PV modules, these components are not included in the geometry to reduce the complexity of the model. Secondly, the material properties of each layer are defined and presented in Table 3.2. These layers of PV modules are subjected to changes in temperature due to their thermophysical properties.

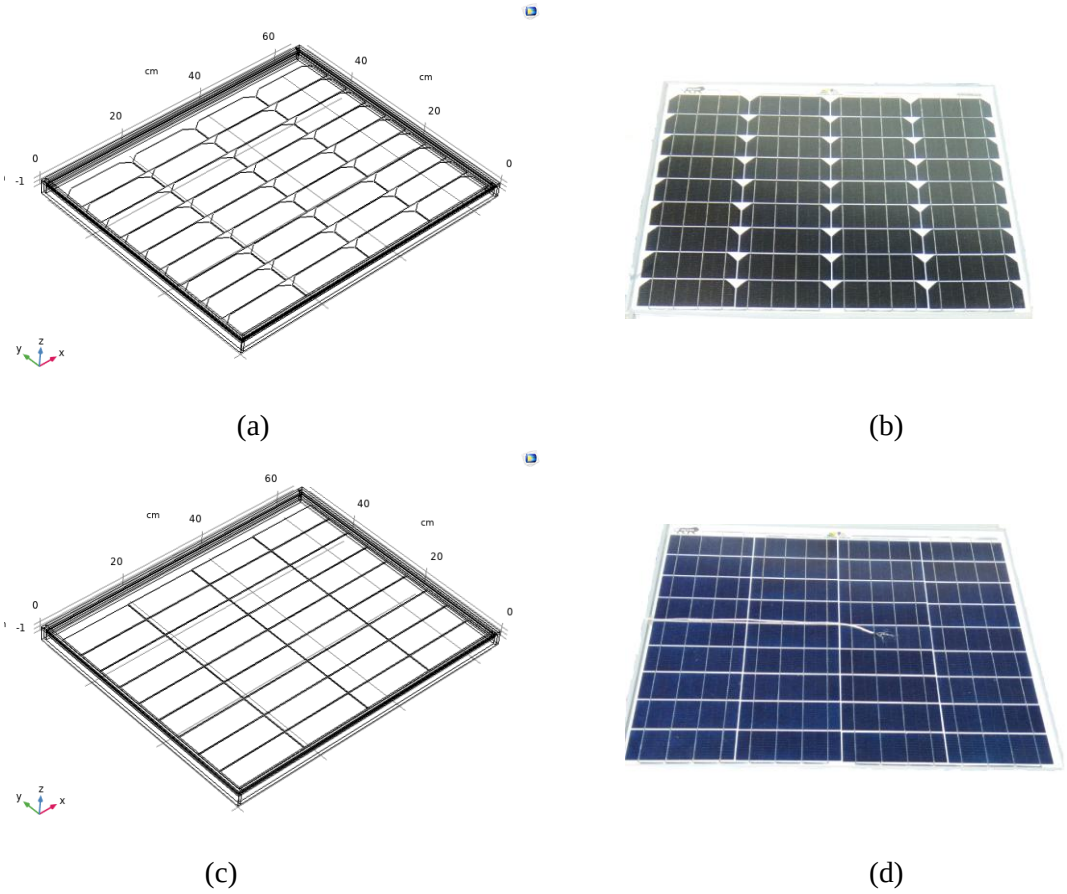

Figure 3.8 (a) Geometry of the modeled m-Si PV module, (b) photograph of the m-Si PV module, (c) geometry of the modeled p-Si PV module, and (d) photograph of the p-Si PV module.

Table 3.2 Thermophysical properties and dimensions of the materials.

Material	***k* (W/m.K)**	**ρ (kg/m^3)**	**c_p (J/kg.K)**	***L* (cm)**	***B* (cm)**	***x* (cm)**
Glass	1.38	2203.00	480.00	64.80	53.00	0.32
EVA	0.29	935.00	2400.00	64.80	53.00	0.10
Silicon cell	130.00	2329.00	700.00	15.60	5.20	0.03
Backsheet	0.14	1200.00	1250.00	64.80	53.00	0.05
Aluminum	238.00	2700.00	900.00	Outer side layer of the module		

Note: k = thermal conductivity, ρ = density, c_p = heat capacity at constant pressure, L = length, B = breadth, and x = thickness.

In the next step, the boundary conditions are set, and the solar cells are considered as the heat source. The heat flux (in power) obtained using equation (3.9)

is used in the heat source (solar cell). Assumptions considered for maintaining simplicity in the thermal model are as follows:

- No contribution of dust deposition or other agents on the absorption of the incident solar spectrum on the PV module.
- The incident solar spectrum (G), wind speed (W_s), relative humidity (RH), and ambient temperature (T_{amb}) are uniformly distributed boundary conditions.
- Heat transfer between the layers and between the surfaces and surroundings is considered via conduction, convection, and radiation heat transfer.
- The gap between each layer of the PV module is ignored because the gaping size is comparatively small with respect to the overall size of the module.

The model is developed using the heat transfer module in solids, and the governing equation is as follows [223]:

$$\rho c_p \left(\frac{\partial T}{\partial t} + u_{trans} \cdot \nabla T \right) + \nabla \cdot \left(q + q_r \right) = Q_{ted} + Q \qquad (3.12)$$

where ρ is the density, c_p is the heat capacity at constant pressure. T is the temperature (K), u_{trans} is the translational motion velocity vector (m/s). q and q_r are the heat flux by conduction and radiation (W/m^2), respectively. Q is the additional heat source (W/m^3), and Q_{ted} is the thermoelastic damping (W/m^3).

Heat transfer in the PV module occurs via conduction, convection, and radiation. Conduction heat transfer takes place between different layers of the module, and conductive heat transfer (q_{cond}) can be equated as:

$$q_{cond} = -k\, A \frac{dT}{dx} \qquad (3.13)$$

where k is the thermal conductivity (W/m.K), A is the area (m^2), T is the temperature (K), and x is the material thickness (m).

Convective heat transfer takes place between the surface of the module and the surroundings. The convective heat transfer (q_{conv}) is given by:

$$q_{conv} = h_{conv}\, A\, (T_{ext} - T) \qquad (3.14)$$

where h_{conv} is the convective heat transfer coefficient (W/m^2.K). T_{ext} and T are the surrounding ambient and PV surface temperatures (K), respectively. The wind speed affects the convective heat transfer [35]; therefore, in this work, the convective heat transfer coefficient at an instant is calculated using [155, 224]:

$$h_{conv} = 2.8 + 3W_s \tag{3.15}$$

where W_s is the wind speed (m/s).

The radiative heat transfer is expressed by the standard equation given as:

$$q_{rad} = \varepsilon \sigma A (T_{ext}{}^4 - T^4) \tag{3.16}$$

where ε is the emissivity and ε of the front and back surfaces are considered to be 0.91 and 0.85, respectively, and σ is the Stefan Boltzmann constant (5.67×10^{-8} W/m^2.K). The proposed model does not include the calculation of parameters, including Nusselt, Reynolds, and Prandtl numbers that involves additional information of the parameters. This makes the model simple and decreases the parameter or information required to estimate the performance of the PV module. Next, the geometry is discretized into smaller sub-division, and user-controlled tetrahedral meshing has been defined for the whole geometry designed as shown in Figure 3.9. The maximum element size, minimum element size, maximum element growth rate, curvature factor, and resolution of the narrow region are 4.6, 0.174, 1.58, 0.6, and 0.5, respectively, for the m-Si PV module and 5, 0.187, 0.155, 0.4 and 0.7, respectively for the p-Si PV module.

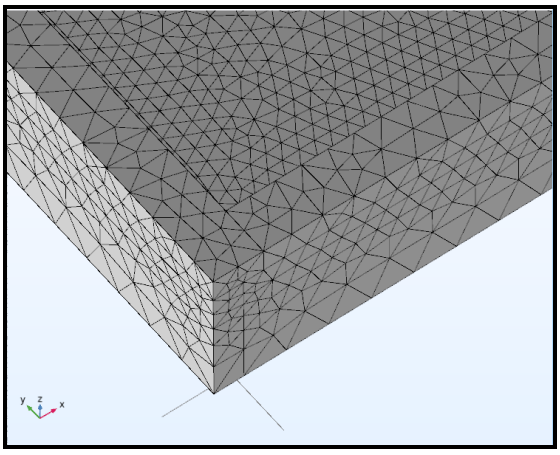

Figure 3.9 Mesh structure of PV module.

Finally, the transient study with time step (initial time, step interval, final time) has been set for the computation step, where the prerequisite parameters like time have been set for a time-dependent study. The time-stepping method Backward Differentiation Formula (BDF) is used as a solver with free steps and the maximum and minimum BDF order being 2 and 1, respectively.

The thermal model outputs the temperature distribution in each layer of the PV module, and most importantly, the instantaneous cell temperature of the module is obtained, which is then fed to the electrical model along with the varying solar spectrum. Therefore, a more precise estimation of the power output from the electrical model can be achieved.

3.1.3 Electrical modeling

The spectrum-based electrical model has been developed using MATLAB to analyze the electrical output of the PV module. The basic electrical equations governed in the solar cell are used along with the electrical parameters provided by the manufacturer. The one-diode model of a PV circuit with series and shunt resistance is used in the modeling as because of its good accuracy level and simplicity [107], and its circuit diagram is shown in Figure 3.10.

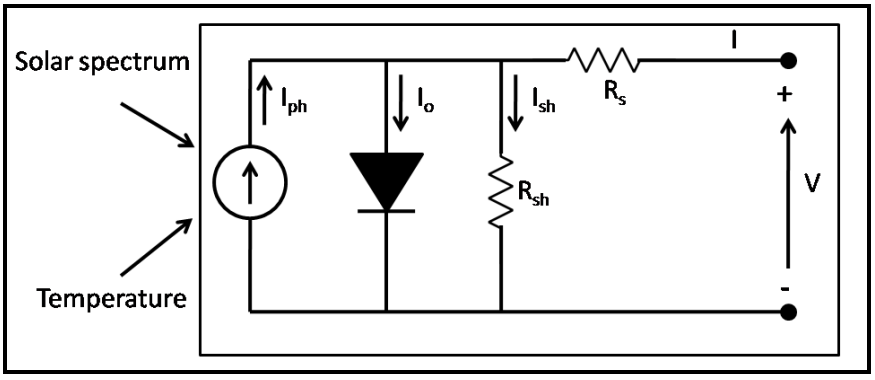

Figure 3.10 PV circuit diagram consisting of one-diode, series, and shunt resistance with solar spectrum and temperature as input parameters.

The electrical parameters which are not provided by the manufacturer are determined using the current-voltage equation of solar cell under short-circuit, open-circuit, and maximum point conditions. Since the current-voltage (*I*-*V*) in equation

(3.17) is a complex non-linear equation, it becomes difficult to solve it analytically. Thus, numerical methods are used to solve such equations.

$$I = I_{ph} - I_o\left[\exp\left(\frac{V + IR_s}{nN_sV_{th}}\right) - 1\right] - \frac{V + IR_s}{R_{sh}} \tag{3.17}$$

where I_{ph} is the photocurrent generated by the PV module (A), I_o is the diode reverse saturation current (A), n is the ideality factor, N_s is the number of cells connected in series, and V_{th} is the thermal voltage (V). R_s and R_{sh} are the series and shunt resistances (Ω), respectively.

Under short-circuit conditions, the current of the PV module is given by [105, 122] :

$$I_{sc} = I_{ph} - I_o\left[\exp\left(\frac{I_{sc}R_s}{nN_sV_{th}}\right) - 1\right] - \frac{I_{sc}R_s}{R_{sh}} \tag{3.18}$$

Under maximum power point (MPP) conditions, the I-V relationship of the PV module is given as:

$$I_{mp} = I_{ph} - I_o\left[\exp\left(\frac{V_{mp} + I_{mp}R_s}{nN_sV_{th}}\right) - 1\right] - \frac{V_{mp} + I_{mp}R_s}{R_{sh}} \tag{3.19}$$

where I_{mp} and V_{mp} are a notation for current (A) and voltage (V) obtained at the maximum power point, respectively.

The series and shunt resistances are determined by the slope of the I-V curve at the open-circuit and short-circuit conditions, respectively. The intermediate values of shunt resistance R_{shn} and series resistance R_{sn} can be calculated as [122] :

$$R_{shn} = R_{sho} - R_s \tag{3.20}$$

$$R_{sn} = \frac{V_{oc}R_{so} + nN_sV_{th}\left(R_{sho} - R_{so}\right) - I_oR_{so}R_{sho}}{V_{oc} - I_{sc}R_{sho}} \tag{3.21}$$

where R_{sho} and R_{so} are the initial shunt and series resistances, respectively. V_{oc} is the open-circuit voltage (V).

The ideality factor n can be obtained by:

$$n = \frac{V_{mp} + I_{mp} R_s - V_{oc}}{V_{th} N_s \ln\left[\frac{I_{sc}(R_s + R_{sh}) - I_{mp}(R_s + R_{sh}) - V_{mp}}{I_{sc}(R_s + R_{sh}) - V_{oc}}\right]} \quad (3.22)$$

After the substitution of the R_s value from equation (3.20) and R_{sh} value from equation (3.21) on equation (3.22), n can be re-expressed as:

$$n = \frac{V_{mp}(V_{oc} - I_{sc}\ R_{sho}) + n\ N_s\ V_{th}\ I_{mp}(R_{sho} - R_{so}) + I_{mp}\ V_{oc}\ R_{so} - I_{mp}\ I_{sc}\ R_{so}\ R_{sho} - V_{oc}(V_{oc} - I_{sc}\ R_{sho})}{N_s\ V_{th}(V_{oc} - I_{sc}\ R_{sho}) \ln\left[\frac{I_{sc}\ R_{sho} - I_{mp}\ R_{sho} - V_{mp}}{I_{sc}\ R_{sho} - V_{oc}}\right]} \quad (3.23)$$

Under the varying environmental factors, primarily spectral irradiation (G) and temperature (T), and incorporating the dynamic nature of these parameters, at short-circuit conditions, the current of the PV module is given by [105, 122] :

$$I_{sc}(G,T) = I_{ph}(G,T) - I_o(T)\left[\exp\left(\frac{I_{sc}R_s(G)}{nN_sV_{th}}\right) - 1\right] - \frac{I_{sc}R_s(G)}{R_{sh}(G)} \quad (3.24)$$

The modified equation for I_{ph} is given by-

$$I_{ph}(G,T) = (I_{ph,n} + K_i\Delta T)\frac{\int_{\lambda_1}^{\lambda_2} G_o(\lambda)EQE(\lambda)d\lambda}{\int_{\lambda_1}^{\lambda_2} G_{AM1.5}(\lambda)d\lambda} \quad (3.25)$$

where $\Delta T = T_c - T_r$, T_c is the cell temperature obtained from the 3D thermal model, and T_r is the reference temperature (°C). K_i is the temperature coefficient for short-circuit current (A/°C). λ_1 and λ_2 are the initial and final wavelength (nm) ranges, respectively, and $G_{AM1.5}$ is the standard ASTM G173-03 AM1.5 spectrum [225].

$$I_{ph,n} \approx \frac{R_s + R_{sh}}{R_{sh}} I_{sc} \quad (3.26)$$

$$I_o(T) = \frac{I_{sc} - K_i(T_c - T)}{\left[\exp\left(\frac{V_{oc} - K_v(T_c - T)}{nN_s V_{th,n}}\right) - 1\right]} \tag{3.27}$$

here $V_{th,n} = k_B T/q$, k_B is the Boltzmann's constant (1.38×10^{-23} J/K), q is the electronic charge (eV), and K_v is the temperature coefficient of open-circuit voltage (V/°C).

The series and shunt resistances are in inverse linear relation with solar irradiance [226]. Therefore, the equations of R_s and R_{sh} can be written as-

$$R_s(G) = \frac{R_{sn} \int_{\lambda_1}^{\lambda_2} G_{AM1.5}(\lambda) d\lambda}{\int_{\lambda_1}^{\lambda_2} G_o(\lambda) EQE(\lambda) d\lambda} \tag{3.28}$$

$$R_{sh}(G) = \frac{R_{shn} \int_{\lambda_1}^{\lambda_2} G_{AM1.5}(\lambda) d\lambda}{\int_{\lambda_1}^{\lambda_2} G_o(\lambda) EQE(\lambda) d\lambda} \tag{3.29}$$

The open-circuit voltage, V_{oc}, as a function of spectral irradiance and temperature, is calculated using-

$$V_{oc}(G,T) = V_{oc} + K_v \Delta T + nN_s V_{th} \ln \frac{\int_{\lambda_1}^{\lambda_2} G_o(\lambda) EQE(\lambda) d\lambda}{\int_{\lambda_1}^{\lambda_2} G_{AM1.5}(\lambda) d\lambda} \tag{3.30}$$

Thus, the obtained electrical parameters are used to calculate the power output of the PV technologies using the equation given by-

$$P_{max} = V_{oc} \cdot I_{sc} \cdot FF = I_{mp} \cdot V_{mp} \tag{3.31}$$

where P_{max} is the maximum power (W), and FF is the fill factor and is 0.77 (derived from the electrical specifications provided by the manufacturer at Standard Test Conditions).

The spectrum-based thermal model and electrical model are integrated using the COMSOL Multiphysics MATLAB Livelink module. Therefore, we obtain the overall electrical parameters I_{sc}, $V_{oc,}$ and P_{max} using equations (3.24), (3.30), and (3.31), respectively, under the varying diurnal solar spectrum and cell temperature.

3.2 Effect of soiling on photovoltaic module

In this work, soiling effect on the PV modules is investigated using a few glass coupons are considered as the proxy to the front glass surface of the PV module and using PV modules. The flow of methodology is shown in Figure 3.11. This section of work consists of three parts: In the first part, the weekly transmittance of proxy glass coupons with different cleaning cycles has been used to obtain the seasonal correlation between the soiling and the environmental parameters using linear regression model. In the second part, the weekly transmittance of proxy glass coupons with different cleaning cycles has been used to determine the effectiveness of different cleaning cycles using statistical analysis (F-test and t-test).

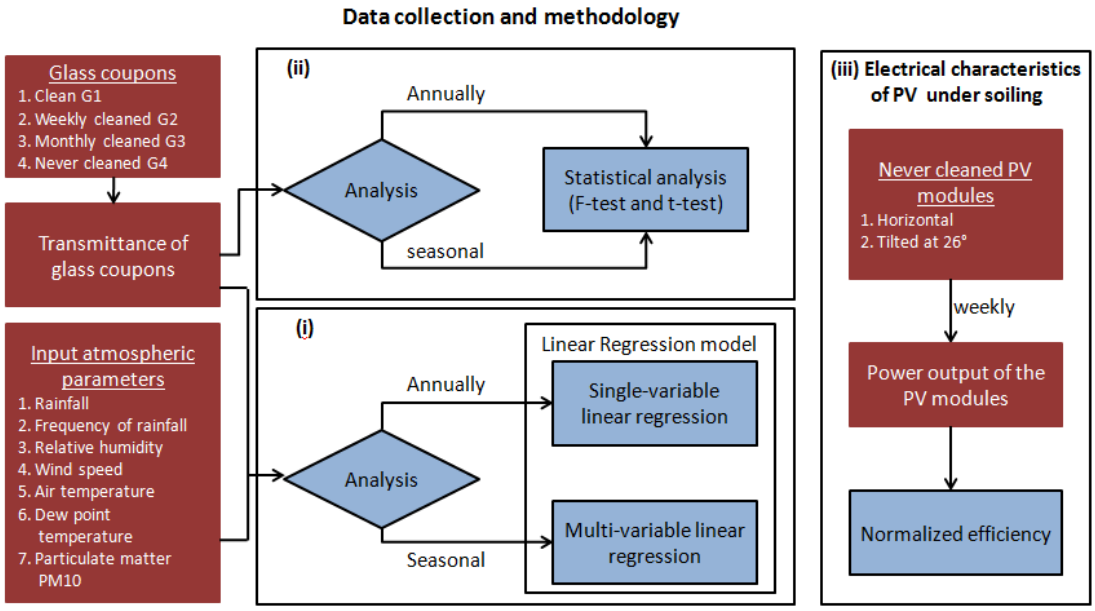

Figure 3.11 Flowchart of the novel methodology that can: (i) evaluate the variability of soiling and its seasonal correlations with environmental factors using the linear regression models, (ii) assess the effectiveness of the different cleaning cycles using the statistical t-test analysis, and (iii) evaluate the electrical characteristics of the PV module under soiling.

Thirdly, PV modules were placed outdoors at 0° and 26° inclinations without any manual cleaning to investigate the electrical characteristics and the decrease in efficiency of the PV module due to soiling. The details are explained in the next subsections.

3.2.1 Location description

The methodology presented in this work is validated with outdoor data collected in Tezpur, Assam (latitude 26.62° North and longitude 92.79° East), on the northern bank of the river Brahmaputra in North-East India. The location has a warm temperate climate with a dry winter, hot summer, and high humidity (Cwa category as per the Köppen-Geiger climate classification) [227]. This designation applies to locations as diverse as Busan, South Korea; Lucknow, India; Zhengzhou, China; Hong Kong; Lilongwe, Malawi; Mackay, Queensland; Santiago del Estero, Argentina; and Guadalajara, Jalisco, Mexico. The Köppen-Geiger climate classification across the world [228] is shown in Figure 3.12.

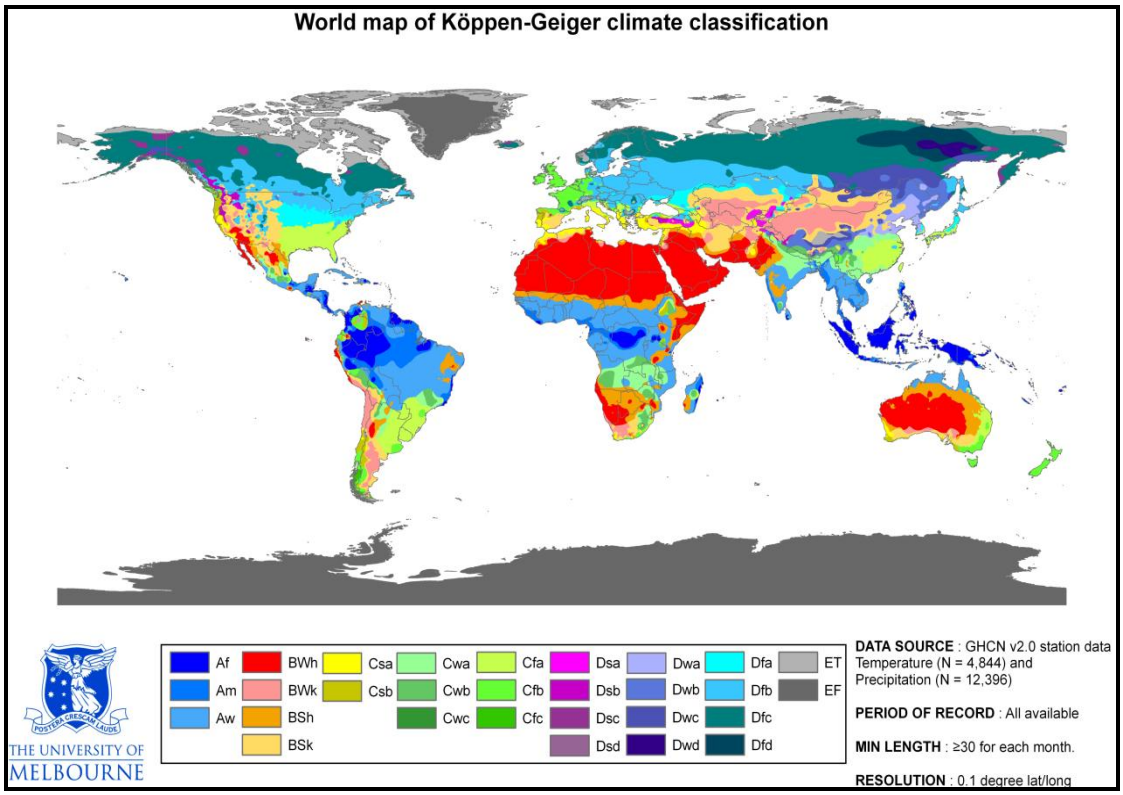

Figure 3.12 The Koppen-Geiger climate classification [228].

The location falls under the Eastern Himalayan region of the Agro-climatic zone in India and receives average global insolation below 4 kWh/m^2/day annually [229]. The experiments are conducted within the Tezpur University campus (10 km from Tezpur), basically, a rural area where households use biomass such as wood, bamboo, crop residues, cow dung, and, occasionally, charcoal for cooking and heating purposes [230]. The nearby area is occupied by residences, subtropical deciduous trees, and agricultural land. This part of the country experiences four distinct seasons: Winter (January and February), Pre-monsoon (March to May), South-west (SW) monsoon (June to October), and Post-monsoon (November and December) [231, 232].

3.2.2 Environmental parameters

The seasonal change in the environmental parameters that could be observed throughout the year is depicted in Figure 3.13. The week number in this study starts from the week in which the experiment is initiated, and it is not related to the week of the year. The environmental parameters such as rainfall intensity, wind speed, relative humidity, and ambient air temperature are measured at 1-minute intervals by a weather station (Station: Tezpur University, under the National Institute of Wind Energy, India) installed near the experimental site. The values of environmental parameters in Figure 3.13, rainfall intensity, relative humidity (*RH*), wind speed (W_s), and air temperature (T_{amb}), are the weekly average of the data collected every minute. There are many ways to sum and analyze the basic mm/minute data for rainfall. The average weekly rainfall intensity (*Rain*) in Figure 3.13 is the direct average of rainfall in mm/minute registered over the week × 60 minutes × 24 hours. The highest value for *Rain* occurred during the SW monsoon (19.7 mm/day), with pre-monsoon (13.0 mm/day), post-monsoon (3.0 mm/day), and winter (1.9 mm/day) being the lowest. The maximum hourly rainfall intensity (R_{max}) is the maximum rainfall of the cumulative rainfall over an hour. The rainfall value recorded in mm/minute is summed for each hour of the week, and the maximum value among them is the maximum weekly rainfall. The frequency of rainfall is denoted by R_f, which is the number of days with rainfall each week. The R_f fluctuates between 0 and 7 days per week during the SW monsoon, while there are just 0 to 3 days per week during the winter. In winter, an extended dry period of up to 28 days has been recorded (i.e., the

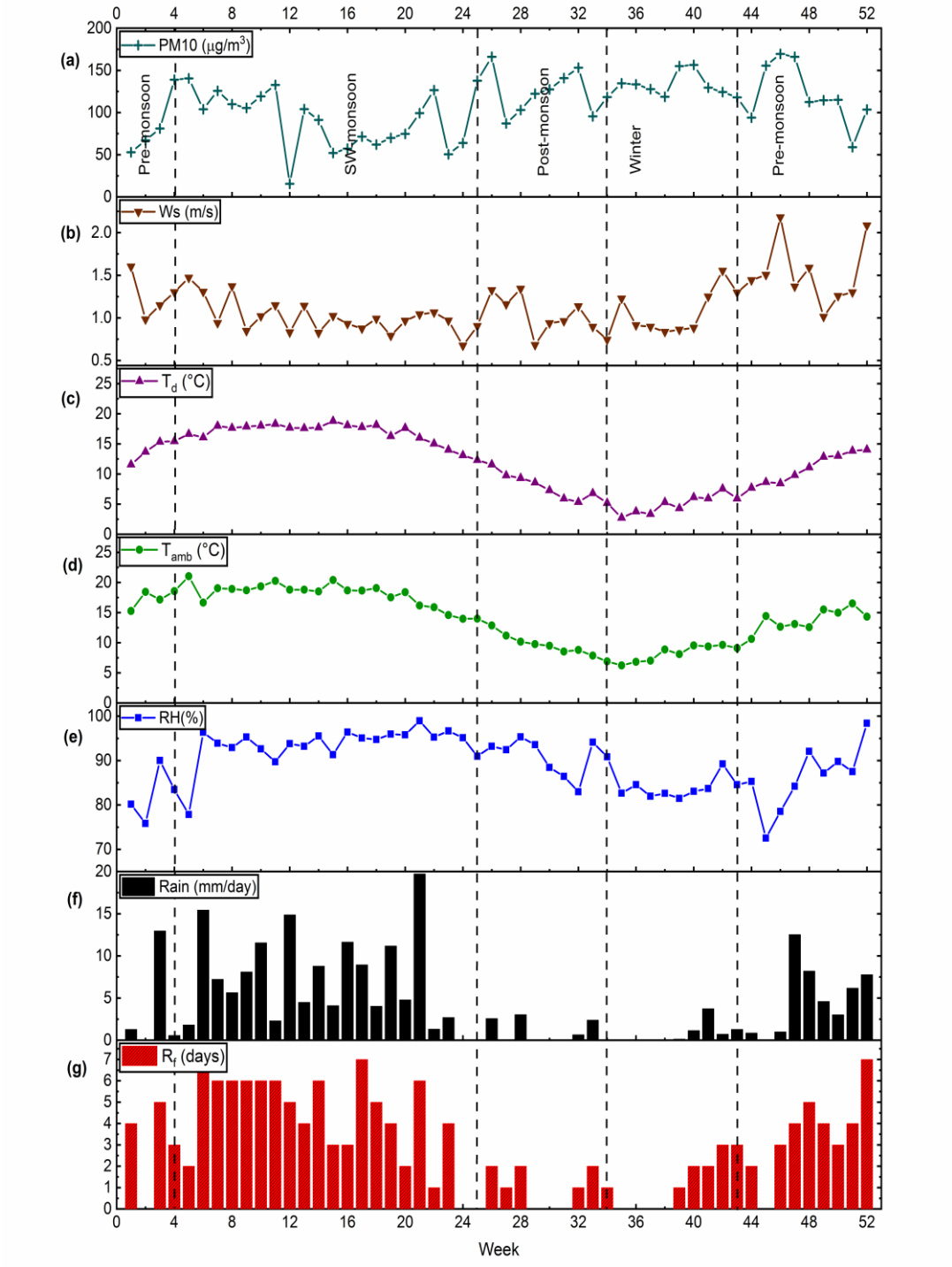

Figure 3.13 The average weekly value of the environmental parameters (a) particulate matter, *PM10* (µg/m^3), (b) wind speed, W_s (m/s), (c) dew point temperature, T_d (°C), (d) ambient air temperature, T_{amb} (°C), (e) relative humidity, *RH* (%), and (f) rainfall intensity, *Rain* (mm/day), which is equal to the direct average, over a given week, of the rainfall recorded in mm per minute multiplied by 60 minutes × 24 hours; (g) weekly frequency of rainfall R_f (days).

weeks between 35 and 38). R_f is extremely high during SW monsoon, gradually fall during the post-monsoon and winter, then rises again during pre-monsoon; this cycle is typical for the area under study. Weekly mean value of particulate matter concentrations are obtained from the Pollution Control Board, Department of Environment and Forest, Government of Assam (Station: Tezpur- 536). The average weekly particulate matter (*PM10*) is the direct average over the week. The *PM10* concentration recorded is 135 µg/m^3 during winter and 128.5 µg/m^3, 107.8 µg/m^3, and 95.3 µg/m^3 during post-monsoon, pre-monsoon, and SW monsoon, respectively. The *RH* for a year lies in the range of 70-98%, depending on the intensity and frequency of the rainfall. It is relatively low during the winter (84.4%), and during the SW monsoon, it is at its maximum (93.2%).

The average weekly air temperature (T_{amb}) during the pre-monsoon and SW monsoon season is high and gradually decreases from post-monsoon to winter season. T_{amb} during pre-monsoon season ranges from 9°C to 18°C, SW monsoon ranges from 14°C to 21°C, post-monsoon season ranges from 8°C to 13°C, and winter ranges from 6°C to 10°C. The dew formation on the PV surface is one of the parameters that can influence soiling [55]. Dew point temperature (T_d) is calculated using the August-Roche-Magnus Equation [233]:

$$T_d = \frac{d\gamma}{b-\gamma} \tag{3.32}$$

where b = 17.67 and d = 243.5°C. The γ is given by,

$$\gamma = \ln\left(\frac{RH}{100}\right) + \frac{bT_{amb}}{d+T_{amb}} \tag{3.33}$$

The average weekly dew point temperature (T_d) during the SW monsoon, post-monsoon, winter, and pre-monsoon seasons are 16.7°C, 8.1°C, 4.9°C, and 11.2°C, respectively.

Table 3.3 Distribution (percentage of total days) of wind speed for each of the four seasons.

Wind speed (m/s)	SW monsoon (%)	Post-monsoon (%)	Winter (%)	Pre-monsoon (%)
0-2	87.8	85.2	84.8	74.4
2-4	11.7	14.4	14.1	22.8
4-6	0.5	0.4	1.1	2.7
6-8	<0.1	-	<0.1	0.1
8-10	-	-	-	<0.1
10-12	-	-	-	<0.1

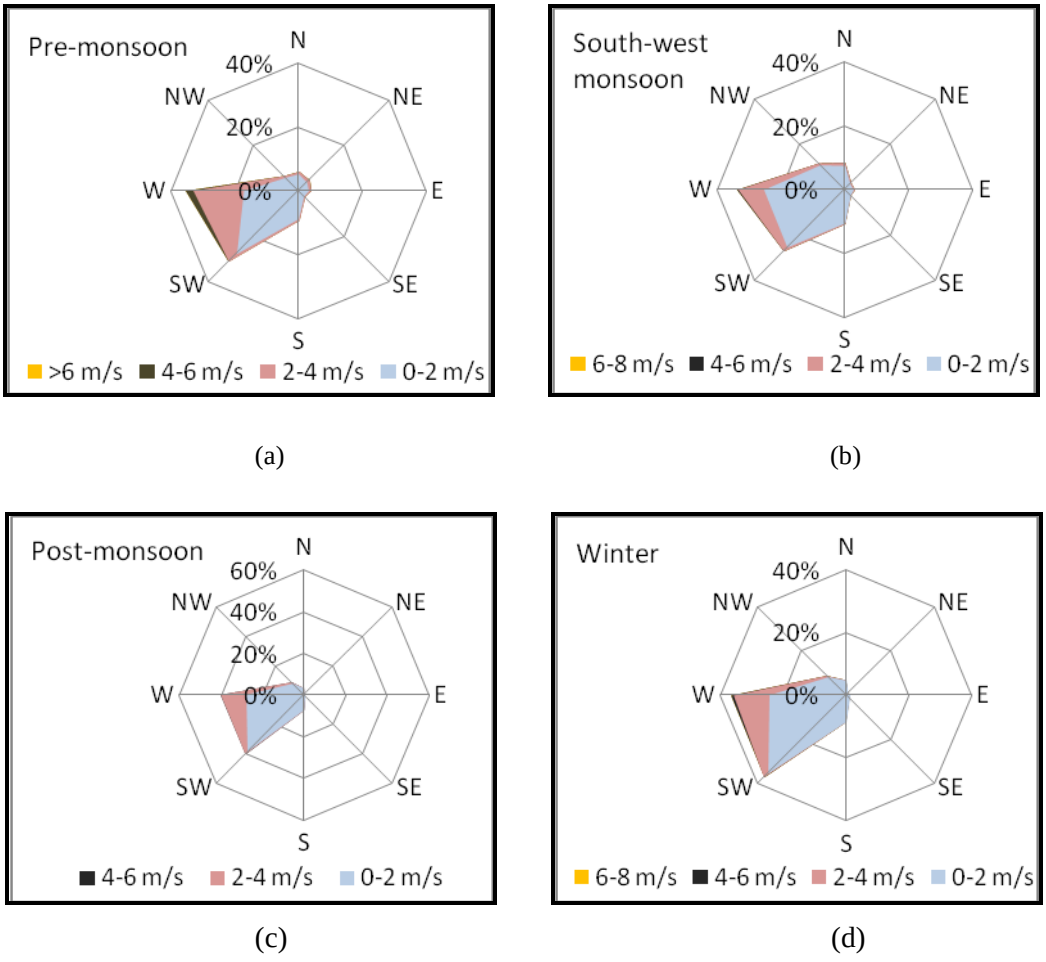

Figure 3.14 Rose diagram for the wind direction of (a) pre-monsoon, (b) SW monsoon, (c) post-monsoon, and (d) winter seasons at the test site in Tezpur, India.

The total percentage contributions for different ranges of W_s, summed from all directions during the various seasons, are presented in Table 3.3 and Figure 3.14. Higher wind speed values have been observed during the pre-monsoon season, with maximum instantaneous wind speed values up to 12 m/s, resulting in a 2.2 m/s weekly

average wind speed (W_s) during the season. The maximum percentage of the wind (22.8%) within the range of 2-4 m/s irrespective of direction is also experienced in this season, one that has a higher tendency to deposit dust onto a surface [4]. The average weekly wind speed (W_s) higher than 6 m/s is extremely rare, i.e., <0.1% of the occurrences in all the seasons. The wind having the lowest speed mostly flows from the west and south-west direction, whereas east and north-east winds flow with the highest wind speed.

3.2.3 Transmittance of the glass coupons

The soiling on the PV surface can be analyzed using the transmittance measurement of the front glass surface. This analysis can enhance the performance and energy yield of the PV module as it can provide the percentage of loss associated with soiling.

3.2.3.1 Measurement of transmittance

Four low iron glass coupons of dimension 4 cm × 4 cm with 3 mm thickness are used in this study. Out of which three are mounted horizontally in an open rack at a 1.5 m height (Figure 3.15) and one of them is kept clean.

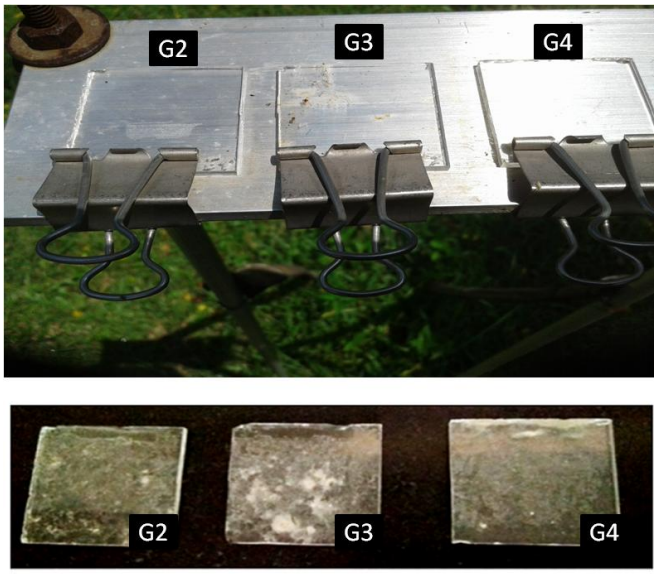

Figure 3.15 Photographs of the glass coupons placed outdoors having different cleaning cycles, weekly cleaned (G2), monthly cleaned (G3), and never cleaned (G4) (above), and an example of the non-uniform distribution of soiling observed, for example, at week 45 (below).

The glass coupons are numbered as follows: G1 (reference glass, kept clean inside a sealed box), G2 (cleaned weekly), G3 (cleaned monthly), and G4 (never cleaned). Cleanings are performed using water and a microfiber cloth. The coupons are exposed to outdoor conditions from May 2018 to May 2019. The direct spectral transmittance of these glass coupons is measured weekly in the 350-1000 nm wavelength range with a 1 nm increment. A UV-Vis spectrophotometer (UV-10) with VISONlite SCAN mode is used, as shown in Figure 3.16. UV-Vis spectrophotometer is an instrument that uses UV-Vis spectroscopy analytical technique. A sample is illuminated with light that spans the UV-Vis wavelength range using a light source in a UV-Vis spectrophotometer. At each wavelength, the device then measure the amount of light that the sample absorbs, transmits or reflects. The main components of a spectrophotometer are a light source that radiates electromagnetic energy in UV-Vis regions of the spectrum, a dispersion device where wavelengths are separated from the broadband radiation, an area designated for sampling through which light is directed or reflected, and one or more detectors to gauge the intensity of radiation either reflected or transmitted. Additional optical components that relay light through the device includes mirrors, lenses, and fiber optics [234].

Figure 3.16 Photograph of the UV-Vis spectrophotometer used in transmittance measurement of the glass coupons.

The use of horizontal orientation for glass coupons is standard practice in the study of soiling [180]. Horizontal orientation can allow for more facile and direct comparisons across different sites and often provides the maximum possible rate of

soiling for the fundamental studies that are the focus of this work. The deposition velocity utilized in the first principle (ab initio) soiling models is parallel to the force of gravity and normal to the horizontal plane [235]. In addition, solar panels installed on many flat roofs for commercial systems are tilted at less than 5° to maximize power density per unit area and minimize shading losses between the rows [236]. The direct spectral transmittance of all the glass coupons is measured before the installation and during the experimental campaign at weekly intervals. The measured direct transmittance of each glass coupon is normalized to the direct transmittance of the clean glass [180, 237]. In this way, the impact of the transmittance of the glass is eliminated. The relative direct spectral transmittance $\tau_r(\lambda)$ is expressed as:

$$\tau_r(\lambda) = \frac{\tau_{soiled}(\lambda)}{\tau_{clean}(\lambda)} \tag{3.34}$$

where $\tau_{soiled}(\lambda)$ and $\tau_{clean}(\lambda)$ are the weekly measured direct spectral transmittance of the soiled and clean glass coupons, respectively.

3.2.3.2 Ångström turbidity

The aerosol present in the atmosphere attenuates the light is represented by the Ångström turbidity equation. Empirically, the transmittance τ of a column of air as a function of wavelength, based on the Ångström turbidity equation is as follows:

$$\tau(\lambda) = \exp(-b\ \lambda^{-a}\ m) \tag{3.35}$$

where m is the air mass.

The Ångström turbidity equation considers both scattering and absorption by the particles. A study [180] sampled accumulation of soiling at seven locations worldwide having different climatic and environmental conditions. It has been reported that the transmittance value of spectral characteristics of soiled surface is lower in the UV and blue visible regions of the spectrum and increases steadily towards the red visible region and infrared region of the spectrum.

As one of several quality checks for the transmittance data, the weekly τ_r versus wavelength is checked against the modified Ångström turbidity equation [180]. As a quality control, the relative spectral transmittance curves are checked against the

modified Ångström turbidity equation. This modified Ångström turbidity equation is found to represent the transmittance of atmosphere which includes the aerosols and particulate matter and is given by [180]:

$$\tau(\lambda) = \exp(-b\,\lambda^{-a}) + c \qquad (3.36)$$

where a and b are the parameters connected to the size and the surface coverage of the particles, respectively. The parameter c is an offset parameter. The selected boundary conditions for the parameters a, b, and c and the fit to equation (3.36) are:
$0.01 < a < 5$, $0 < b < 0.5$, and $-0.35 < c < 0.1$
The soiling transmittance loss of exposure is calculated for each week as [180, 237]:

$$\tau_{loss} = (1 - \tau_r) \qquad (3.37)$$

The average relative direct transmittance, τ_r, is the simple average over the wavelength range 350-1000 nm of the spectral transmittance averaged using three spots on the glass coupon. The broadband direct spectral transmittance (wavelength range 350-1000 nm) of the clean glass is 0.91. This work uses τ_r and τ_{loss} of soiled glass to investigate cleaning strategies and the correlation between the transmittance due to soiling and several key environmental parameters.

3.2.4 Statistical linear regression models

Both the single-variable linear regression (SLR) and multi-variable linear regression (MLR) models have been used to correlate the environmental parameters to the transmittance of the glass coupon. In this model, the dependence of the transmittance of the glass coupon on the considered individual environmental parameters is investigated. The Microsoft Excel regression analysis tool is used for linear curve fitting. The transmittance of the glass coupon is considered a linear function of the environmental parameter(s) and is expressed as:

$$\tau_r = \alpha_0 + \alpha v \text{ (single variable)} \qquad (3.38)$$

where α_0 is the intercept, v is the environmental parameter's value, and α is its coefficient. Similarly, MLR is expressed as:

$$\tau_r = \alpha_0 + \alpha_1 v_1 + \alpha_2 v_2 + \alpha_3 v_3 + \ldots + \alpha_n v_n \text{ (multiple variables)} \qquad (3.39)$$

where α_0, α_1, α_2, α_3,…, α_n are the intercept and the variables' coefficients and v_1, v_2, v_3,…, v_n are the input environmental parameters.

The p-value and R^2 are used to quantify the quality of the regression. The p-value describes the significance of the relationship, and the R^2 value indicates the degree to which the dependent variable is explained by the model [238]. The input parameters of the correlation are considered significant if the p-value < 0.05. The model used combinations of the environmental parameters to estimate the weekly transmittance of glass coupon G2.

3.2.5 Electrical characteristics of PV module under soiling

Three PV modules are placed outdoors at different orientations: horizontally (0°), tilted (26°, latitude of the location under study). These PV modules are from the same manufacturer and have the same electrical specifications; the electrical specifications are depicted in Table 3.4. The experimental setup was installed on 24th November 2020, and the experiment was carried out till 15th March 2022. Here, all the seasons in the area are covered in the study, weeks 1-5 and 49-56 are post-monsoon, weeks 6-13 are winter, weeks 14-25 are pre-monsoon, and weeks 29-48 are monsoon. The photograph of the soiling module exposed to natural soiling placed horizontally for 21st week is shown in Figure 3.17. The modules are allowed to undergo natural soiling without any cleaning cycle. The electrical parameters (I_{sc}, V_{oc}, I_{mp}, V_{mp}, and P_{max}) of these modules were measured on a weekly basis using a Solar IVe curve tracer.

To compare the electrical characteristics of the PV module with the transmittance of the glass coupon, an experimental campaign was conducted using another set of low iron glass coupons placed at horizontal and tilted positions. These glass coupons have dimensions (length: 5 cm, breadth: 5 cm, and width: 0.4 cm) and are placed outdoors adjacent to the experimental PV modules. No cleaning is carried out on the glass coupons. The transmittance of the glass coupons is measured using the Shimadzu UV-1700 Spectrophotometer for the wavelength range 300-1000 nm. A set of six measurements are taken at different points of glass for each glass coupon.

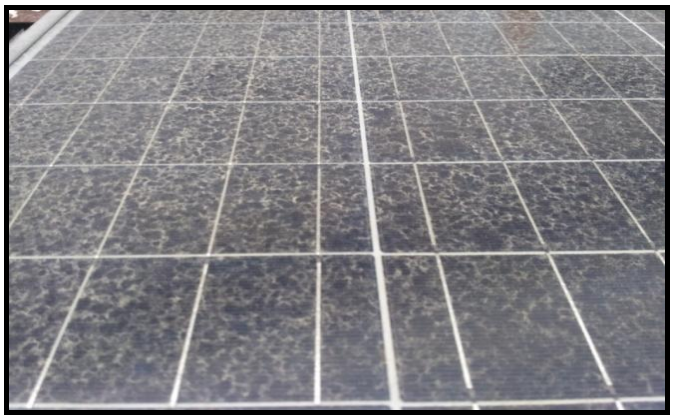

Figure 3.17 The photograph of the horizontally placed PV modules under the soiling.

Table 3.4 Specifications of the p-Si PV module used in the experimental setup to investigate the soiling effect.

Polycrystalline solar PV module- MTK50/12V	
Parameter	**Value (Unit)**
Power wattage (P_{max})	50.00W
Short-circuit current (I_{sc})	3.06 A
Open-circuit voltage (V_{oc})	21.90 V
Maximum current (I_{mp})	2.78 A
Maximum voltage (V_{mp})	17.96 V
Area	0.30 m^2

The efficiency of the soiled module is normalized using the data recorded on the initial day of the experiment due to the non-availability of measurements of the electrical characteristics of the clean module on a respective day. The normalized efficiency is calculated using equation (3.40):

$$\eta_{normalized} = \frac{P_{soiled} / P_{initial}}{G_{soiled} / G_{initial}} \tag{3.40}$$

where P_{soiled} is the power output of the soiled PV module, and $P_{initial}$ is the power output of the clean PV module (measured on the day of installation when the modules are clean). G_{soiled} and $G_{initial}$ are the plane of array irradiance of the soiled PV module and clean module (measured on the installation day), respectively.

Moreover, depending on the incident solar irradiance and the PV technology (for specification, see Table 3.4, the power output of a PV module changes with soiling. The energy yield loss from a PV panel due to soling is calculated as follows:

$$E_{loss} = E_{clean} - E_{soiled} \tag{3.41}$$

where E_{clean} is the energy yield from PV with no soiling, and E_{soiled} is the energy yield from PV with soiling. Further,

$$E_{clean} = P_{clean}\ H_s \tag{3.42}$$

$$E_{soiled} = P_{soiled}\ H_s \tag{3.43}$$

where P is the power output and subscripts *soiled* and *clean* are for PV modules with soiling and without soiling, respectively. H_s is the sunshine hour. The location has, on average 9 sunshine hours in the pre-monsoon and SW monsoon seasons and 8 hours for the post-monsoon and winter seasons [239]. The power output is expressed as:

$$P = J_{sc}\ r_s\ V_{oc}\ FF \tag{3.44}$$

where J_{sc} is the short-circuit current density, V_{oc} is the open-circuit voltage, and FF is the fill factor of the PV module. r_s is the soiling ratio, as defined in [240], here, r_s is 1 for a clean PV module and it decreases with the increase in losses (in equation (3.44)). Indeed, the soiling loss (power loss due to soiling) can be calculated as ($1-r_s$).

Under the assumption of uniformly distributed soiling, the instantaneous soiling ratio at an instantaneous time t can be expressed as:

$$r_s(t) = \frac{J_{sc\_soiled}(t)}{J_{sc\_clean}(t)} \tag{3.45}$$

where $J_{sc\_soiled}(t)$ is the short-circuit current density of the module under natural soiling and $J_{sc\_clean}(t)$ is the short-circuit current density of the clean module. Equation (3.45) can also be expressed as:

$$r_s(t) = \frac{J_{sc\_soiled}(t)}{J_{sc\_clean}(t)} = \frac{\int_{\lambda_2}^{\lambda_1} G_D(\lambda,t)\,\tau_r(\lambda,t)\,SR(\lambda)d\lambda}{\int_{\lambda_2}^{\lambda_1} G_D(\lambda,t)\,SR(\lambda)d\lambda} \qquad (3.46)$$

where λ_1 and λ_2 are the upper and lower limit of the absorption band of the PV material, respectively. $G_D(\lambda,t)$ is the spectral distribution of the solar irradiance (as in Figure 3.18) on the typical day representing the season of a year. $SR(\lambda)$ is the spectral response of the PV material, in this case we have considered p-Si, as shown in Figure 3.18.

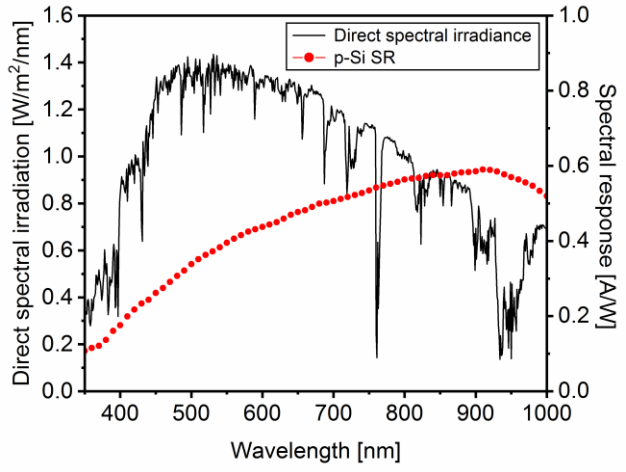

Figure 3.18 Direct spectral irradiance [241] and spectral response of the p-Si considered in evaluation of the electrical performance of the soiled PV module under standard test conditions.

3.3 Statistical approaches for data analysis

Various statistical indices are used to analyze the data obtained from the developed model and measured data. Some of the indices that are used for soiling analysis include standard deviation (*SD*), uncertainty (*u*), coefficient of determination (R^2), and F-test and t-test analysis. The *SD* and *u* of the average relative direct transmittance, τ_r of various glass coupons (G2, G3, and G4) are calculated using equations (3.47) and (3.48), respectively [242]. These values were obtained based on the measurement of direct transmittance of the glass coupons at three different positions (left, center, and right). It is important to calculate the deviation and

uncertainty because soiling has non-uniform distribution on the surface. The statistical F-test and t-test analysis are carried out to determine the statistically meaningful differences in net soiling on a seasonal basis. These tests are performed on the average relative direct transmittance, τ_r of the glass coupons for various seasons to determine the effectiveness of different cleaning cycles (weekly, monthly, and no cleaning). The R^2 value is used to determine the significance of the correlation between the average relative direct transmittance and various environmental parameters obtained from the linear regression models.

A few statistical errors that are commonly used to analyze the predicted data of the spectrum based electrical-thermal model and their experimental dataset are such as R^2, mean absolute error (MAE), mean relative error (MRE), root mean square error (RMSE). These errors determine the prediction level of the developed model in comparison to the experimentally measured parameters. Here, the parameters such as I_{sc}, V_{oc}, P_{max}, and T_c are validated on the basis of these errors. Moreover, the parameter global spectral irradiance generated is also validated based on the R^2 value.

The numerical expression and physical significance of these statistical indices are as follows:

Standard deviation (SD): The standard deviation signifies the deviation of the dataset from its mean value. The equation for standard deviation is given by:

$$SD = \sqrt{\frac{\sum_{i=1}^{r}(X_i - \mu)^2}{(r-1)}} \tag{3.47}$$

where X_i is the i^{th} reading in the dataset, μ is the mean of the dataset and r is the number of readings in the dataset.

Uncertainty (u): The uncertainty expresses the standard deviation of the mean of the dataset.

$$u = \sqrt{\frac{\sum_{i=1}^{r}(X_i - \mu)^2}{r(r-1)}} \tag{3.48}$$

Mean absolute error (MAE): MAE represents the average of the absolute difference between the simulated and measured values of the dataset. It signifies the average of the residuals in the dataset.

$$MAE = \frac{1}{r}\sum_{i=1}^{r}\left|y_{\exp,i} - y_{sim,i}\right| \tag{3.49}$$

where y_{exp} and y_{sim} are the experimental and simulation outputs for i^{th} data, respectively, and r is the number of samples.

Mean relative error (MRE): MRE is the average of the ratio of the mean absolute error of measurement to the measured value of the dataset, which provides the uncertainty of measurement in comparison to the size of the measurement.

$$MRE = \frac{1}{r}\sum_{i=1}^{r}\left|\frac{y_{\exp,i} - y_{sim,i}}{y_{\exp,i}}\right| \tag{3.50}$$

Mean square error (MSE): MSE is defined as the mean of the squared difference between the measured and predicted data; it describes the variance of the residuals. The MSE is expressed as:

$$MSE = \frac{1}{r}\sum_{i=1}^{r}\left(y_{\exp,i} - y_{sim,i}\right)^2 \tag{3.51}$$

Root mean square error (RMSE): RMSE is the squared root of the mean squared error (signifies the variance of the residuals) and represents the standard deviation of the residuals.

$$RMSE = \sqrt{\frac{1}{r}\sum_{i=1}^{r}\left(y_{\exp,i} - y_{sim,i}\right)^2} \tag{3.52}$$

Coefficient of determination (R^2): R^2 measures the percentage of variation in the dependent variable that is predicted by the independent variable.

$$R^2 = 1 - \frac{\sum_{i=1}^{r}\left(y_{sim,i} - y_{\exp,i}\right)^2}{\sum_{i=1}^{r}\left(y_{sim,i} - \bar{y}\right)^2} \qquad (3.53)$$

where $\bar{y}$ is the mean of the *y* value.

Statistical F-test and t-test: The statistical F-test and t-test are based on hypothetical assumptions. These are useful in determining the relationships between the variables and the probability of error that exists if we consider the determined relationship. The F-test null hypothesis states that the two samples have the same variance. The F-test null hypothesis cannot be rejected when the absolute F-statistic is less than the absolute F critical two-tail value, and the p-value is greater than 0.05. If these conditions are not obtained, then the null hypothesis is rejected, and the two samples have statistically different variances. Following the F-test analysis, a t-test with equal variance is performed if the p-value > 0.05, and a t-test with unequal variance analysis is performed if the p-value < 0.05. The t-test null hypothesis states that the mean value of the two samples is equal. The conditions to support the t-test hypothesis is when the t-statistic is less than the absolute t-critical two-tail value, and the p-value is greater than 0.05. The null hypothesis is rejected if these conditions do not meet, and the two samples are said to have different mean values.

3.4 Experimental work for validation of the designed model

An experimental process flow for the performance evaluation of the PV module under varying environmental parameters is discussed. This experimental work is carried out to validate the simulation results from the developed spectrum-dependent electrical-thermal model of the PV module. The energy yield evaluation with and without soiling effect is also presented.

3.4.1 Instruments and experimental setup

The experiment is conducted in the outdoor condition under varying spectral intensity and environmental parameters. Two PV modules: p-Si and m-Si, are mounted in an open rack oriented towards the south at a 26° tilt angle (coordinates of location:

26.7° North and 92.8° East). The electrical specifications of these modules provided by the manufacturer are shown in Table 3.5.

Table 3.5 Specification of the p-Si and m-Si PV modules used in the experimental validation.

Parameters	**p-Si**	**m-Si**
P_{max}	50 W	50 W
I_{sc}	3.1 A	3.1 A
V_{oc}	21 V	21 V
I_{mp}	2.8 A	2.8 A
V_{mp}	17.3 V	17.3 V
NOCT	47°C ± 3%	47°C ± 3%
Tolerance	0±3	0±3
Area	0.299 m^2	0.290 m^2
Number of cells	36	36
NOCT: Nominal operating cell temperature		

The modules are cleaned properly before the experiment to minimize the soiling effect. The schematic of the instruments and their interconnections in the experimental setup is depicted in Figure 3.19. The PV modules are not connected to any load, so the instantaneous electrical outputs are measured from the PV module terminals directly for a representative day of various seasons. The solar spectrum, environmental parameters (T_{amb}, RH, and W_s), surface temperatures, and electrical outputs of the PV modules are measured for a time period of 8:30 to 15:00 at 5 minutes intervals. Noting that the time mentioned in this work is the local time. The environmental parameters, including wind speed and relative humidity, are measured using an anemometer and hygrometer, respectively. The spectral distribution of the solar spectrum is recorded using the Blue-wave Spectrometer mounted near the PV modules in the same rack. The spectrometer has a CR2 cosine receptor which enables it to correctly respond to and measure spectral irradiance, resolutions, and bandwidth 180° field of view. The outdoor experimental setup for validation of simulated results, along with the instruments and their interconnections as presented is Figure 3.18 is shown in Figure 3.20.

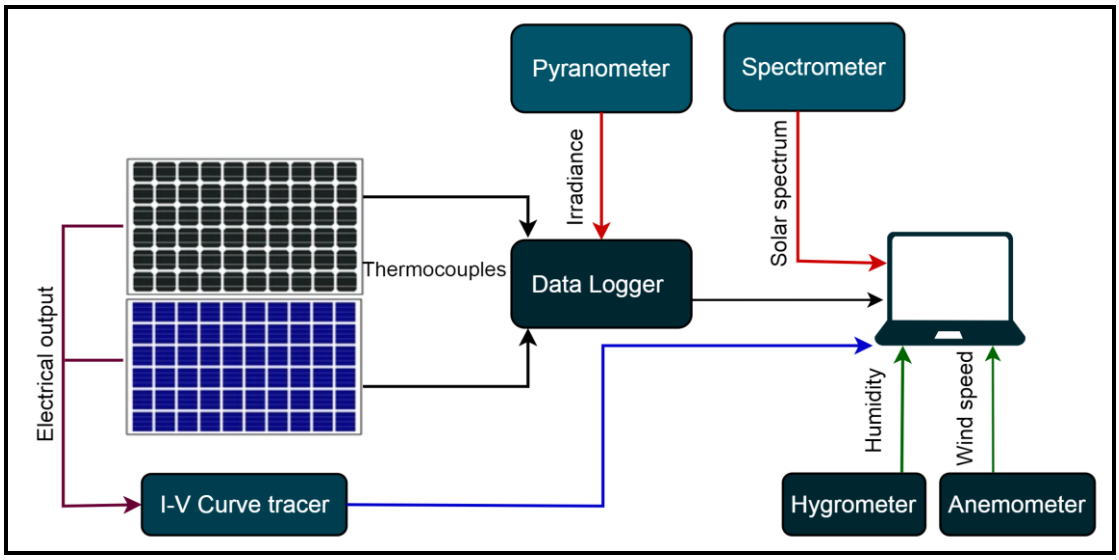

Figure 3.19 Schematic of the experimental setup showing the interconnection between different instruments.

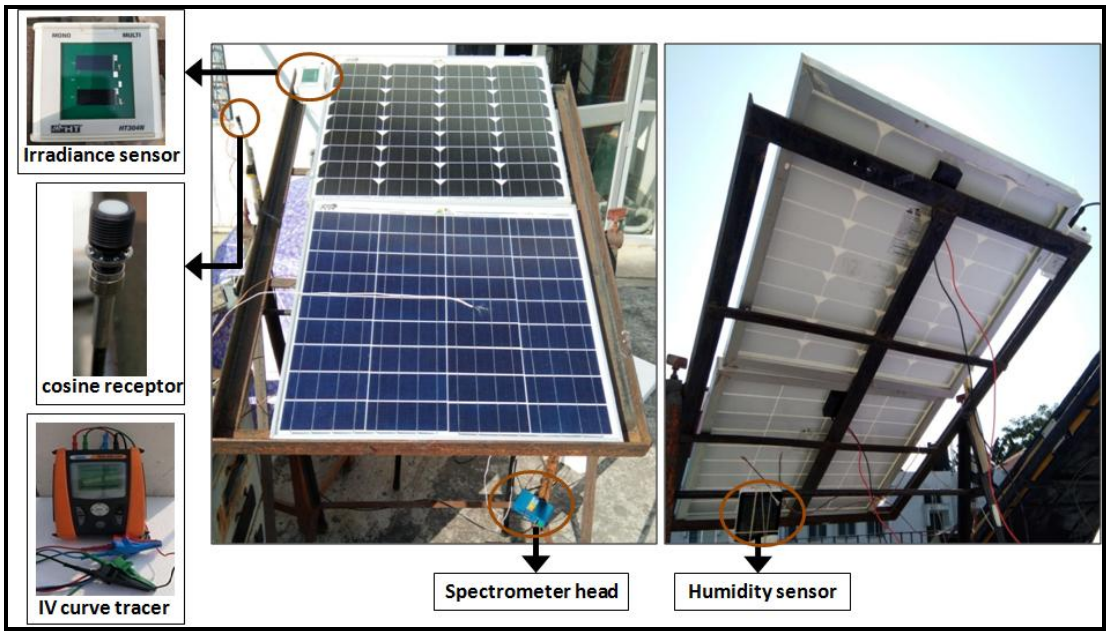

Figure 3.20 Outdoor experimental setup at the Roof of the Department of Energy, Tezpur University, Tezpur, India for validation of the developed integrated spectrum-based model.

Table 3.6 Specification of the instruments used in the experimental validation of the developed models.

Instruments	**Make and Model**	**Range and Accuracy**
Pyranometer CMP6	Kipp and Zonen	285-2800 nm
Blue-wave Spectrometer	StellarNet	200-1150 nm
Solar IVe curve tracer	HT	15-99.9 V, resolution: 0.1
Digital Anemometer	PM6252A Peakmeter	0.8-30 m/s, ±(2.0% reading +50 counts) 0.01 m/s
Hygrometer	HTC-2	10-90%, +3 Rh (50%~80%)

The specifications of the instruments used to measure different parameters are depicted in Table 3.6. The solar irradiation at the horizontal plane is measured using the Kipp and Zonen CMP6 pyranometer. As the sun's position changes with time, the angle between the sun and the fixed tilt surface changes. Therefore, global tilted irradiance can be calculated using the global horizontal irradiance [243]:

$$G_{tiltted} = G_{horizontal} \frac{sin(\alpha + \beta)}{sin\alpha} \tag{3.54}$$

where α and β are the elevation angle, and the PV module tilted angle from the horizontal. The elevation angle α is given by:

$$\alpha = \sin^{-1}(\sin\delta\sin\phi + \cos\delta\cos\phi\cos\omega) \tag{3.55}$$

where φ is the latitude, and δ is the declination equation (3.7). ω is the hour angle and is given by:

$$\omega = 15°(LST - 12) \tag{3.56}$$

where LST is the local solar time given by: $LST = LT + \frac{TC}{60}$ (3.57)

where LT is the local time. TC is the time correction factor (in minutes) and is expressed as:

$$TC = 4(Longitude - LSTM) + EoT \tag{3.58}$$

where local standard time meridian (*LSTM*) and equation of time (*EoT*) are calculated using the equations:

$$LSTM = 15(LT - UTC) \tag{3.59}$$

$$EoT = 9.87sin2B_o - 7.53cosB_o - 1.5sinB_o \tag{3.60}$$

where *UTC* is the universal coordinated time (in hours), and B_o (in degrees) is expressed as:

$$B_o = (d - 81)\frac{360}{365} \tag{3.61}$$

where d is the i^{th} day of the year.

The surface temperatures (front and back) along with the ambient temperature, are measured using a temperature sensor (K-type thermocouples), and these data are recorded using the Agilent 34972A data logger. Since, the real-time cell temperature (T_c) within the PV module is complicated to be measured directly using a thermocouple, therefore, the same is calculated using indirect method using the back surface temperature the following equation [161]:

$$T_c = T_b + \frac{G_{exp}}{G_r}\Delta T_o \tag{3.62}$$

where T_b is the temperature of the back surface of the PV module (°C), and ΔT_o is the temperature difference between the cell and the back surface at reference solar irradiance, considered as 3°C (typical value for flat-plate module type glass/cell/back sheet mounted in a open-rack). G_{exp} is the measured solar irradiance (W/m^2), and G_r is the reference solar irradiance (1000 W/m^2). The electrical output (I-V and P-V characteristics) of the PV modules are measured using the Solar IVe curve tracer. The experiments are conducted on various days of the season under clear-sky conditions, and for the validation, a typical day of the season is considered.

3.4.2 Energy yield

The energy yield of the PV module obtained from the simulation and experiment is calculated and compared for various seasons of the year. The energy yield of a PV module for a day is calculated using equation (3.63):

$$E = \sum_{t=t_i}^{t_f} P_t \; H_s \tag{3.63}$$

where P_t is the power output at time *t.* t_i and t_f are the initial and final times of the day, respectively.

The typical energy yield (calculated using equation (3.63)) obtained from the developed model is validated using the measured energy yield for the considered seasons. Earlier, in section 3.2.5 we have described the energy loss in PV due to soiling under standard test conditions. However, to further investigate the energy yield of the soiled PV modules under varying solar spectrum and environmental conditions, equation (3.1) can be rewritten as follows:

$$G_{o\_soiled} = G \; \tau \; \tau_r \tag{3.64}$$

Using equation (3.64), the part of spectral irradiance that contributes to electricity generation under soiling conditions is obtained from the developed model (in section 3.1). Here, the average τ_r value measured for various seasons with three cleaning cycles (weekly, monthly, and never cleaned) is used to evaluate the energy yield for respective conditions. Therefore, the seasonal energy yield of the PV modules is calculated considering the typical representative day of the season, considering the methodology in sections 3.1 and 3.3.

3.5 Summary

In this chapter, the process flow of work for development of spectral, thermal, and electrical model is discussed. Here, the details of the dimension, orientation and cleaning pattern or cycle of the installed glass coupons to study the effect of soiling on PV module is provided. Also, the specifications of the components in the experimental setup are given. The methods, measurements and data analysis techniques used to obtain the objectives of this research work is also discussed.